Polish Society of Composite Materials
Polskie Towarzystwo Materiałów Kompozytowych

24: 2 (2024) 141-154

COMPOSITES THEORY AND PRACTICE

ISSN (online): 2299-128X

D. Sarukasan*, K. Thirumavalavan

Anna University, Department of Mechanical Engineering, CEG Campus, India
**Corresponding author. E-mail: saru31kasan@gmail.com*

Received (Otrzymano) 03.03.2024

INVESTIGATION OF MECHANICAL AND DEGRADATION CHARACTERISTICS OF FILAMENT-WOUND COMPOSITE PIPES INCORPORATING BASALT/E-GLASS HYBRID REINFORCEMENT

https://doi.org/10.62753/ctp.2024.09.2.2

This study investigates the mechanical (flexural and low-velocity impact test) and chemical (immersion degradation test) properties of basalt/E-glass hybrid fiber-reinforced polymer composite pipes (HFRP) fabricated by the filament winding technique. The HFRP composites composed of eight layers at constant fiber tension and the constant winding angle of ±55° for the basalt fiber and ±90° for the E-glass fiber were fabricated employing a 3-axis filament winding machine with a stage by stage curing process in the furnace. Eleven HFRP composite arrangements with fiber content proportions of 100 %, 25:75 %, 50:50 % and 75:25 % and various stacking sequences were studied. The study revealed that the fiber content ratio had a moderate influence on the mechanical properties, while the stacking sequence played a more significant role. Notably, the specific configuration designated as BGH7, which combined 50 % basalt fibers with 50 % E-glass fibers in a particular stacking order, exhibited superior performance. BGH7 demonstrated a remarkable 39.2 % increase in flexural strength compared to the E-glass FRP composite. Additionally, it showed improved resistance to low-velocity impacts at different energy levels: 60.52 % improvement for 20 J, 5.684 % for 30 J, and 21.30 % for 40 J. The BGH7 configuration also displayed superior resistance to chemical degradation. Compared to the E-glass pipes, BGH7 showed a significant improvement in withstanding exposure to NaCl by 33.48 %, HCl by 70.21 %, and H_2SO_4 by 114.78 %. This research suggests that the arrangement of basalt and E-glass fibers, particularly the BGH7 configuration, can significantly enhance the mechanical and chemical resistance of HFRP pipes compared to using E-glass fibers alone. The damage analysis was carried out using scanning electron microscope (SEM) and ultrasonic scan techniques.

Keywords: **composites, basalt fiber, filament winding technique, multi-layer hybrid composite, fractography analysis, ultrasonic scanning analysis**

INTRODUCTION

Underground structures encompass a diverse range of entirely or partially submerged architectural formations, regardless of their geometric configuration. Among these subterranean constructions, cylindrical structures such as pipelines, passageways, tunnels, storage containers and more, have found a variety of applications, serving purposes of spanning water transportation, hazardous fluid conveyance, sewage management, and others [1]. In recent times, there has been a notable increment in the adoption of fiber-reinforced plastic (FRP) pipes. This trend can be primarily attributed to the diminishing cost disparity between FRP pipes and conventional piping systems. FRP pipes offer numerous advantages when juxtaposed with traditional steel pipes. One of the primary drivers for the appeal of FRP pipesresides in their low density, which is approximately one-fourth of that of steel. This distinctive attribute proves particularly advantageous in scenarios where the deployment of heavy handling equipment poses challenges due to spatial constraints, as encountered in underground mining operations [2]. In addition to the weight advantage, FRP pipes offer a gamut of additional benefits compared to traditional steel pipes, encompassing enhanced corrosion resistance, reduced coefficients of thermal expansion, a remarkable strength-to-weight ratio, diminished friction characteristics, and a more user-friendly bonding system [3].

The evolving landscape of energy pipeline construction necessitates a deeper understanding of the real-world implications associated with deformable pipe materials. In a manner akin to the scrutiny applied to most metallic systems, it is imperative to assess the suitability of fiber-reinforced plastic (FRP) pipe materials in this context [4]. Among these materials, basalt fiber emerges as a naturally occurring mineral fiber sourced from basaltic volcanic rock, boasting an array of exceptional attributes. They include remarkable mechanical strength, resistance to high temperatures, outstanding chemical durability, robust resistance to moisture, non-combustibility, and a non-toxic nature.

It is precisely these virtues that have propelled basalt fibers into service as a reinforcement element within polymer matrix composites. It is worth noting that in comparison to E-glass fiber, basalt fiber exhibits a higher density, albeit at a relatively higher cost [5-8].

The application of basalt fiber-reinforced plastic (BFRP) piping systems introduces a wide array of distinctive characteristics that surpass those of stainless steel and have a profound impact on various design properties. Furthermore, these systems exert a considerable influence on the surrounding soil conditions within subterranean structures [9]. In the quest to fully comprehend the properties of BFRP pipes, substantial research efforts have been channeled into investigating the mechanical behavior of composite pipes under load. Hybrid composites, designed to harness the advantages of their constituent materials while mitigating some of their inherent limitations, have been a focal point in this research endeavor [10]. The utilization of different types of fibers in a hybrid configuration has emerged as a successful strategy for reducing the inherent ductility limitations observed in composite materials. Hybridization serves as a mechanism to introduce progressive failure in composites, thereby yielding more cost-effective materials. The amalgamation of fibers can be achieved through various configurations, including intermingled, intra-mingled, and sandwiched layers. By incorporating robust natural fibers into these hybrids, it becomes feasible to surmount the limitations and enhance the overall strength, stiffness, and moisture resistance of the composite [11, 12].

Pandian et al. conducted a study investigating the mechanical properties of basalt fiber-reinforced plastic (FRP) composite laminates exposed to alkaline and acid solutions. The results indicate that the interfacial region of the basalt composite is vulnerable to damage caused by hydrolysis. While the tensile and flexural strength were relatively unaffected by water immersion, H_2SO_4 exposure had a discernible impact on the basalt fiber laminates [13]. In a separate investigation, Koutsomichalis et al. fabricated hybrid composite laminates utilizing Kevlar, aluminum/glass, and Vectran materials, with a focus on comparing their flexural behavior. The hybridization of the laminates led to a progressive failure mode, and the Vectran hybrid composite laminate exhibited the highest bending strength among the tested laminates [14]. Muñoz and García-Manrique explored eco-friendly flax fiber-reinforced green composites with varying weight fractions (40 % and 55 %) produced using the resin transfer molding technique. The study centered on evaluating the tensile and flexural properties of specimens immersed in water and comparing them to dry composite specimens. The findings revealed that the flax fiber maintained favorable mechanical properties even when exposed to humid environments, rendering it suitable for potential applications in such conditions [15]. Furthermore, Chen et al. investigated the flexural properties of hybrid FRP composite laminates comprising carbon, basalt, and glass fibers, fabricated using the VARTM process. The results suggested that increasing the basalt fiber hybrid ratio up to 50 % resulted in a decrease in the flexural characteristics, while further raising it to 75 % had no significant impact. Symmetrically placing carbon layers on both the tensile and compressive sides yielded a higher flexural modulus, and higher flexural strength was achieved with a sandwich-like stacking sequence featuring a hybrid ratio of 50 % incorporating basalt or glass fibers [16]. Moreover, Chen et al. delved into the effect of hybrid carbon, glass, and basalt FRP laminates in a sandwich-like stacking arrangement fabricated by means of the VARTM technique, subjecting them to low-velocity impact analysis. The results revealed that placing carbon layers on the exterior resulted in relatively poor impact resistance due to the brittle nature of the carbon fiber. In contrast, the glass and basalt fiber layers displayed similar behavior under low-velocity impact conditions [17]. Sujon et al. conducted an experimental study on jute/carbon hybrid composites, exploring four distinct stacking sequences and three different fiber orientations. Their investigation encompassed an examination of the response of hybrid fiber-reinforced plastic composite laminate to various mechanical loading conditions and its water absorption characteristics. The outcomes of their research demonstrate the superior performance of the hybrid composites in comparison to the angle-ply and cross-ply hybrid composites. While the stacking sequence exerts a noticeable influence on the tensile strength and water absorption properties of hybrid composites, its impact on the flexural and impact characteristics of these materials is even more pronounced. These findings underscore the potential of these hybrid composites as lightweight materials well-suited for load-bearing structural applications [18]. In a related study, Tashnizi et al. reported on cylindrical carbon fiber-reinforced plastic (CFRP) composite pipe laminates, emphasizing the use of a $\phi 55°$ optimal winding angle and appropriate stacking sequence. Their investigation revealed that these composite pipes exhibited enhanced mechanical strength when subjected to patch-loading scenarios [19]. Farhood et al. delved into the impact damage resistance of basalt-carbon hybrid FRP pipes, exploring variations in the fiber content and stacking sequence. Their findings underscored the substantial impact of the stacking sequence on the impact resistance, with the fiber content ratio playing a partial role. Notably, the placement of basalt fiber within the laminate was found to have a significant influence on the impact resistance. Incorporating 50 wt.% and 75 wt.% basalt fiber contents resulted in peak load values, reduced damage areas, and lower energy absorption during impact events [20]. In a separate investigation, Zhang et al. examined the low-velocity impact behavior of carbon-glass intralayer hybrid composite laminates at varying energy levels. They conducted

impact tests and subsequently analyzed the damage area using C-scan techniques and SEM analysis. The results indicated that the carbon-E-glass stacked FRP hybrid structures outperformed the E-glass fiber composite laminates, exhibiting significantly improved performance in low-velocity impact scenarios [21].

In this study, hybrid pipes were manufactured by combining basalt and glass fibers as reinforcement elements, along with an epoxy matrix, using the filament winding technique. The research aimed to thoroughly investigate the impact of key parameters such as the fiber content ratio, fiber winding angle, and stacking sequence of the fibers, through a range of mechanical tests including three-point flexural testing, low-velocity impact assessment, and immersion degradation testing. To measure the extent of impact-induced damage and deformation in the composite laminates, an A-C scan measuring system was employed for precise results. Additionally, the morphological effects of immersion degradation on the composite pipe specimens were examined using scanning electron microscopy (SEM). This comprehensive approach allowed thorough assessment of the performance and structural integrity of the hybrid pipes under different conditions and loading scenarios.

MATERIALS AND METHODS

In the fabrication of the multi-layered hybrid composite pipes in this study, continuous unidirectional roving was employed as the reinforcement material. Specifically, basalt and E-glass fibers were selected as the reinforcement components, and these materials were sourced from Aerotex and Sai Sakthi Pvt. Ltd. The matrix resin chosen for this purpose was Araldite bisphenol-A epoxy resin, which was combined with Aradur HY951 hardener. Additionally, a peroxide acid solution served as the catalyst, and it was also supplied by Sai Sakthi Chemicals. To ensure optimal bonding between the composites, a resin-hardener mixing ratio of 2:1 was maintained, and the mixing process was carried out for a duration of 30 minutes. This meticulous preparation method was employed to achieve strong and reliable bonds within the composite materials. Further details regarding the properties of the utilized fiber and resin materials can be found in Table 1, providing comprehensive insights into their characteristics and specifications.

TABLE 1. **Physical properties of matrix and reinforcement**

Properties	E-glass	Epoxy	Basalt
Density [g•cm^{-3}]	2.58	1.15	2.60
Poisson's ratio	0.35	0.2	0.3
Elastic modulus [GPa]	72	3	93
Tensile strength [MPa]	1970	78	3200

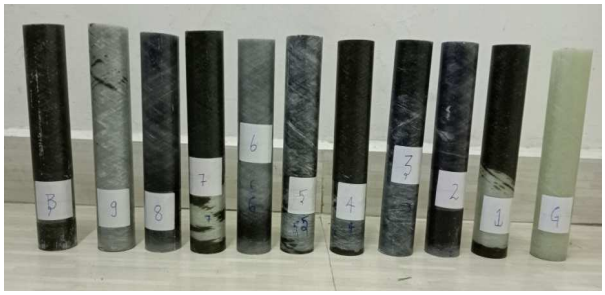

Fig. 1. E-glass, basalt and hybrid FRP composite pipes

The pipe samples were fabricated at Hindustan Industries using the filament winding technique, both in pure and multi-layered hybrid composite configurations. The key factors influencing the process included the winding pattern and stacking sequence, with ±55° for basalt and ±90° for E-glass chosen for the hybrid mixtures. This resulted in superior mechanical strength compared to the conventional ±90° layup with pure E-glass fiber, attributed to the principles of laminate theory. Two categories of pipes were created for examination: one with pure basalt and pure E-glass, and the other with hybrid composites of varying basalt fiber proportions (25 %, 50 %, and 75 %) and stacking sequences. These eleven combinations enable detailed exploration of the mechanical properties and performance characteristics.

The production of the pipes involved utilizing a CNC 3-axis filament winding technique at Hindustan Industries, with the process divided into preparatory, execution, and post-processing stages. A stainless-steel mandrel with a 40-mm inner diameter and 1000-mm length served as the core, undergoing cleaning, polishing, and wax coating for smoothness and easy removal of the produced pipes. Unidirectional fiber roving wound on nylon bobbins was passed through a resin bath and applied to the mandrel during execution. Post-curing in a furnace at 120 °C for 3 hours, then at 150 °C for 2 hours, was followed by cooling and careful mandrel removal [22-24]. The samples were machined to achieve a consistent length-to-diameter ratio of 1:1, with visual inspection for geometrical distortions. Further specifications are given in detail in Table 2.

The evaluation of the flexural properties of the pipe samples involved conducting three-point bending tests, which were carried out using an Instron 6800 series Universal Testing Machine (UTM) equipped with a 300 kN load cell as shown in Figure 2a. These tests took place at the MIT campus in India and adhered to the ASTM D790 standard. During the tests, the pipe specimens, featuring an inner diameter of 40 mm, an outer diameter of 48 mm, and a gauge length of 100 mm along the loading direction, were subjected to a controlled crosshead speed of 2 mm/min^{-1}. This method allowed the generation of force-displacement curves, providing essential data on the flexural strength of the specimens [25, 26].

TABLE 2. **Specification of composite pipes**

Diagram	Notation	Stacking sequence	Thickness [mm]	Outer diameter [mm]	Length [mm
	G_8	G_8	4±0.05	48±0.20	1000
	BGH1	G_6B_2	4±0.05	48±0.20	1000
	BGH2	$G_3B_2G_3$	4±0.05	48±0.20	1000
	BGH3	$B_2G_2B_2G_2$	4±0.05	48±0.20	1000
	BGH4	$B_2B_2G_2G_2$	4±0.05	48±0.20	1000
	BGH5	$G_2G_2B_2B_2$	4±0.05	48±0.20	1000
	BGH6	$G_2B_2B_2G_2$	4±0.05	48±0.20	1000
	BGH7	$B_2G_2G_2B_2$	4±0.05	48±0.20	1000
	BGH8	B_6G_2	4±0.05	48±0.20	1000
	BGH9	$B_3G_2B_3$	4±0.05	48±0.20	1000
	B_8	B_8	4±0.05	48±0.20	1000

Impact behavior testing of the pure and multi-layered hybrid composite pipe samples was conducted at ambient room temperature (30 °C) using the ASTM D7136 standard and a Fractovis Plus drop weight impact testing machine. The fabricated pipes, adjusted using the filament winding technique parameters, were tested with a customized V-shaped fixture and bolt-nut prearranged clamping component as shown in Figure 2b [27]. Three energy levels (20 J, 30 J, and 40 J) were selected to characterize deformation, with three specimens per composite type tested at each energy level. The impacting device, weighing 4.928 kg with a diameter of 12.7 mm, ensured a single impact using a rebound brake mechanism. The specimens were positioned atop a 250 mm long impact support fixture with inner and outer diameters of 40 mm and 48 mm, respectively. This rigorous testing aimed to comprehensively assess the impact resistance and deformation patterns of the materials.

a)

b)

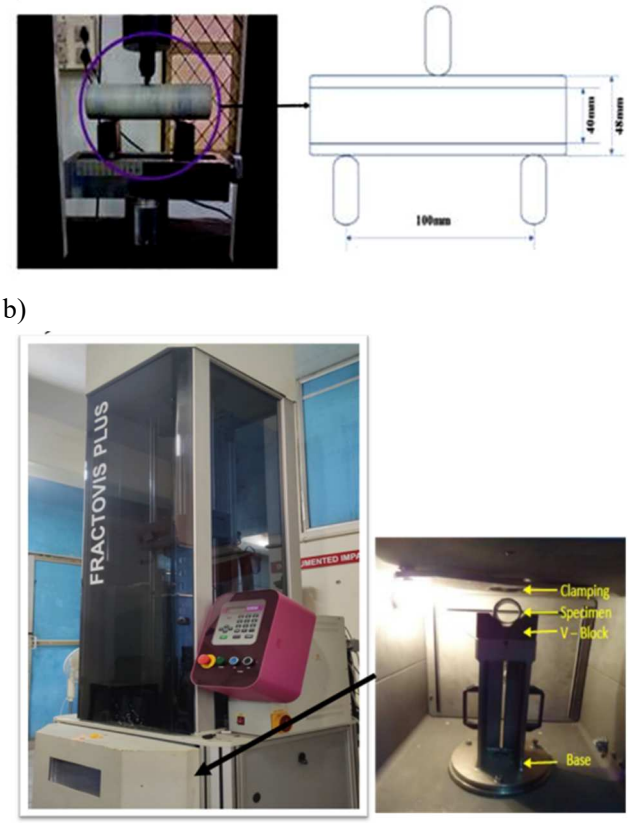

Fig. 2. a) Flexural strength tester, b) Low-velocity impact tester

Non-destructive evaluation of the damaged fiber pipe specimens after low-velocity impact testing was conducted using immersion ultrasonic inspection equipment featuring a 5 MHz frequency transducer (ULTRAPAC UPK-T48-HS apparatus). The study aimed to evaluate the degradation behavior of the E-glass, basalt, and hybrid composite pipe specimens by immersing them in various corrosive environments following ASTM D5229 standards. Standardized composite pipe specimens, 50 mm in length, were immersed in separate containers with different corrosive solutions: 1 M concentrated hydrochloric acid, 95 % pure 0.5 M sulfuric acid, and 3.5 M concentrated sodium chloride (NaCl) solutions. Continuous monitoring over six months included monthly removal for cleaning in an ultrasonic chamber using a Cr_2O_3 and deionized water mixture. After cleaning, the specimens were dried, weighed, and examined at controlled room temperature (30 °C). Weight measurements and parameters such as

moisture absorption and the degradation rate were calculated periodically. Fractographic investigations were performed utilizing a scanning electron microscope (SEM) after sputtering a layer of gold to prevent electrical discharge, allowing comprehensive assessment of material degradation and structural integrity [28].

$$M_L = m_b - m_a \tag{1}$$

$$C_r = \frac{k * M_L}{a \times t \times d} \tag{2}$$

where: M_L – mass loss; M_b, m_a mass before and after immersion; t – time duration; C_r – degradation rate; k = 8.76 · 10^4 constant; a – area (outer surface area + inner surface area + 2 × base area); d = density [g/cm^3].

RESULTS AND DISCUSSION

Flexural behavior

The investigation of the flexural properties of the basalt, E-glass, and their hybrid forms was conducted by means of the three-point flexural test. This test adhered to the ASTM D790 standard, where specimen failure was considered to have occurred when the strain exceeded 5 %. Figure 3 provides a visual representation of the flexural load-displacement curve, demonstrating the variations in the stacking sequences for both the pure and hybrid fiber composite pipes.

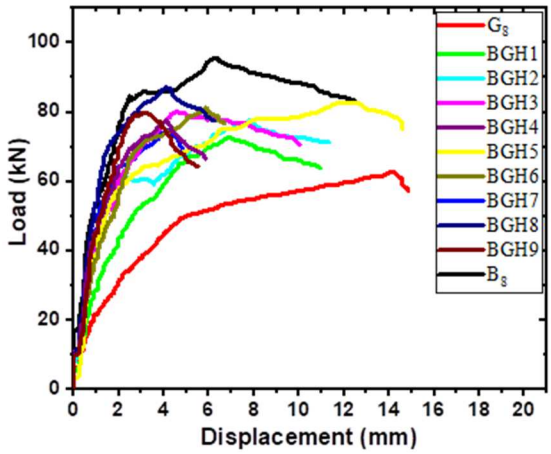

Fig. 3. Flexural properties of pure and hybrid composite pipe

The results presented in Table 3 reveal that the pure E-glass FRP pipes exhibited a flexural strength of 112.94 MPa, followed by the pure basalt FRP pipes at 172.42 MPa. Interestingly, the basalt FRP pipes exhibited a gradual load increase, culminating in a maximum peak load, displaying a brittle mode of failure. Conversely, the E-glass pipes exhibited a peak strength at a lower load increment, accompanied by greater displacement. This observation suggests that the robust elongation characteristics of the basalt fibers contribute to a ductile mode of failure in the composite material. In contrast, the E-glass fibers tend to fail in a different manner, emphasizing the impact of the fiber properties on the structural behavior of the composites.

TABLE 3. **Flexural properties of FRP pipes**

Specimen	Notation	Load [kN]	Displacement [mm]	Flexural strength [MPa]
1	G_8	62.45	14.276	112.94±12
2	BGH1	72.65	10.190	131.39±11
3	BGH2	73.813	10.040	133.49±13
4	BGH3	77.47	8.130	140.11±11
5	BGH4	79.883	7.637	144.474±10
6	BGH5	82.50	7.025	149.207±9
7	BGH6	81.11	6.030	146.965±10
8	BGH7	87.239	6.255	157.77±11
9	BGH8	77.556	5.071	140.266±12
10	BGH9	79.774	4.880	144.277±8
11	B_8	95.337	7.130	172.42±10

In the realm of composite materials, hybridization strategies are employed to not only economize on costs but also to enhance the mechanical properties. In this particular study, a thorough examination was conducted to investigate how the flexural characteristics are influenced by the stacking sequences and modifications in the fabrication process parameters of filament wound pipes (FWP). The hybrid composite pipes denoted as BGH1, BGH2, BGH8, and BGH9, exhibited notable flexural strengths. Specifically, BGH1 and BGH2, featuring a 25 % basalt fiber content, achieved flexural strengths of 131.39 MPa and 133.49 MPa, respectively. On the other hand, BGH8 and BGH9, comprising 75 % basalt fiber, displayed even higher flexural strengths, measuring 140.266 MPa and 144.277 MPa, respectively. The positioning of the basalt fiber layer within the hybrid composite specimens, whether placed on the inner side (BGH1 and BGH8) or in the middle (BGH2 and BGH9), resulted in modest improvement in the flexural strength of these hybrid composite pipe specimens. Furthermore, the hybrid composite samples with the 50 % basalt fiber content, denoted as BGH3 to BGH7, exhibited a range of flexural strengths: 140.11 MPa, 144.474 MPa, 149.207 MPa, 146.965 MPa, and 157.77 MPa. Notably, among the various stacking sequences, BGH7, where the basalt fiber layers were positioned both on the inside and outside of the pipe with E-glass fiber layers in the middle, demonstrated partially linear behavior before reaching the peak load. Consequently, it is advisable to place basalt fiber layers both on the inside and outside of the composite pipe for enhanced flexural resistance in hybrid composites. The findings underscore the advantages of hybridization in composite pipes, particularly when employing diverse stacking sequences and varying fiber contents. Such hybridization strategies consistently yield

improvements in flexural strength when compared to pure E-glass fiber composite pipes.

Degradation behavior

Utilizing an immersion degradation testing technique provides a highly effective means to scrutinize the impact of corrosive environments on fiber composite materials. In the context of this study, immersion degradation testing was employed to assess the degradation behavior of both the pure and hybrid composite specimens when subjected to diverse corrosive solutions such as NaCl, HCl, and H_2SO_4. Figure 4 visually depicts the composite specimens before and after undergoing immersion degradation testing. The exposure of the fiber composites to these chemicals revealed a noteworthy trend: an increase in the level of hybridization of the fiber content within the composites corresponded to a reduction in degradation resistance. This observation underscores the critical role played by the hybridization of fibers in influencing the degradation behavior of these composite materials. It suggests that the incorporation of hybrid fiber compositions may lead to heightened susceptibility to corrosive environments, a crucial consideration in the design and application of such materials in various contexts.

When subjected to exposure to both the alkaline and acidic solutions, an observable mass loss was noted, primarily attributed to the inherent hydrophilic nature of the materials. Figure 5a, b and c graphically represent the variations in the degradation rate and time exposure of the composite specimens immersed in the 3.5 M NaCl [29], 1 M HCl [30], and 0.5 M H_2SO_4 [31] solutions.

These trends are further quantified in Table 4, which presents the mass loss and degradation rate data for the treated pure and hybrid FRP pipe composite specimens. Remarkably, when exposed to the NaCl solution, the pure basalt fiber composites exhibited the smallest mass loss and degradation rate as compared to their pure E-glass fiber counterparts, following approximately six months of exposure. It is worth noting that the hybridization of the basalt and E-glass fibers, accomplished by varying the stacking sequences and process parameters within the filament winding technique, resulted in an enhanced degradation resistance relative to the pure E-glass fiber composites. The progression of demineralization in the fiber composites, namely the pure E-glass, basalt, and their hybrid counterparts, was assessed in H_2SO_4, known for causing the most significant damage, followed by HCl. Notably, HCl caused a decidedly higher degree of demineralization. It was deduced that the presence of highly soluble chloride ions facilitated more accessible interchange reactions between the H+ ions in the acid and ions within the fiber composites. This observation implies that the degradation behavior of the fiber composite pipes in acidic environments follows a demineralization process, where the ions within the composite are initially attacked by H+ ions in the acid on the composite surface. The concentration of H+ ions played a pivotal role in influencing the outcome of this HFRP composite, which suffers from peeling defects in acidic media.

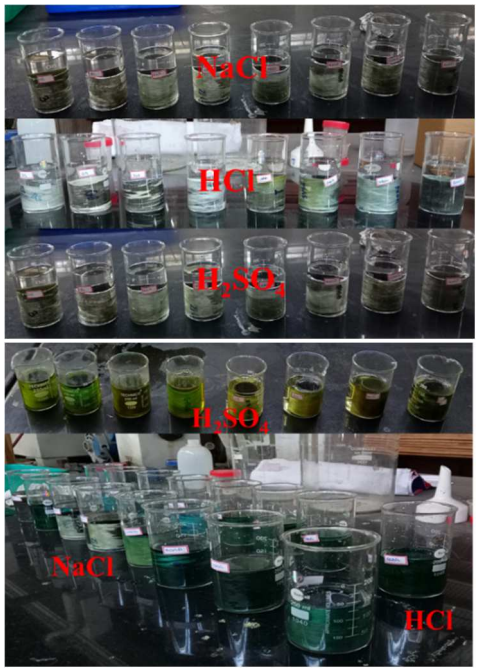

Fig. 4. Composite specimens before and after immersion in degradation test containers

TABLE 4. **Degradation properties of pure and hybrid composite pipe specimens**

Specimen	Notation	NaCl mass loss [g] (M_L)	HCl mass loss [g] (M_L)	H_2SO_4 mass loss [g] (M_L)	NaCl degradation rate [mpy]	HCl degradation rate [mpy]	H_2SO_4 degradation rate [mpy]
1	G_8	0.155	0.203	1.3	0.0548	0.0684	0.4474
2	BGH1	0.142	0.145	0.522	0.0502	0.0512	0.2126
3	BGH2	0.102	0.148	0.344	0.035	0.0508	0.1216
4	BGH3	0.07	0.074	0.148	0.0247	0.0318	0.0637
5	BGH4	0.068	0.085	0.155	0.0239	0.03	0.0548
6	BGH5	0.08	0.121	0.279	0.0325	0.0492	0.0939
7	BGH6	0.066	0.128	0.334	0.0284	0.0349	0.0911
8	BGH7	0.06	0.069	0.126	0.0212	0.0244	0.0445
9	BGH8	0.06	0.067	0.075	0.018	0.0236	0.0265
10	BGH9	0.088	0.071	0.175	0.024	0.0251	0.0618
11	B_8	0.007	0.066	0.082	0.0024	0.0198	0.0246
mpy = mils per year							

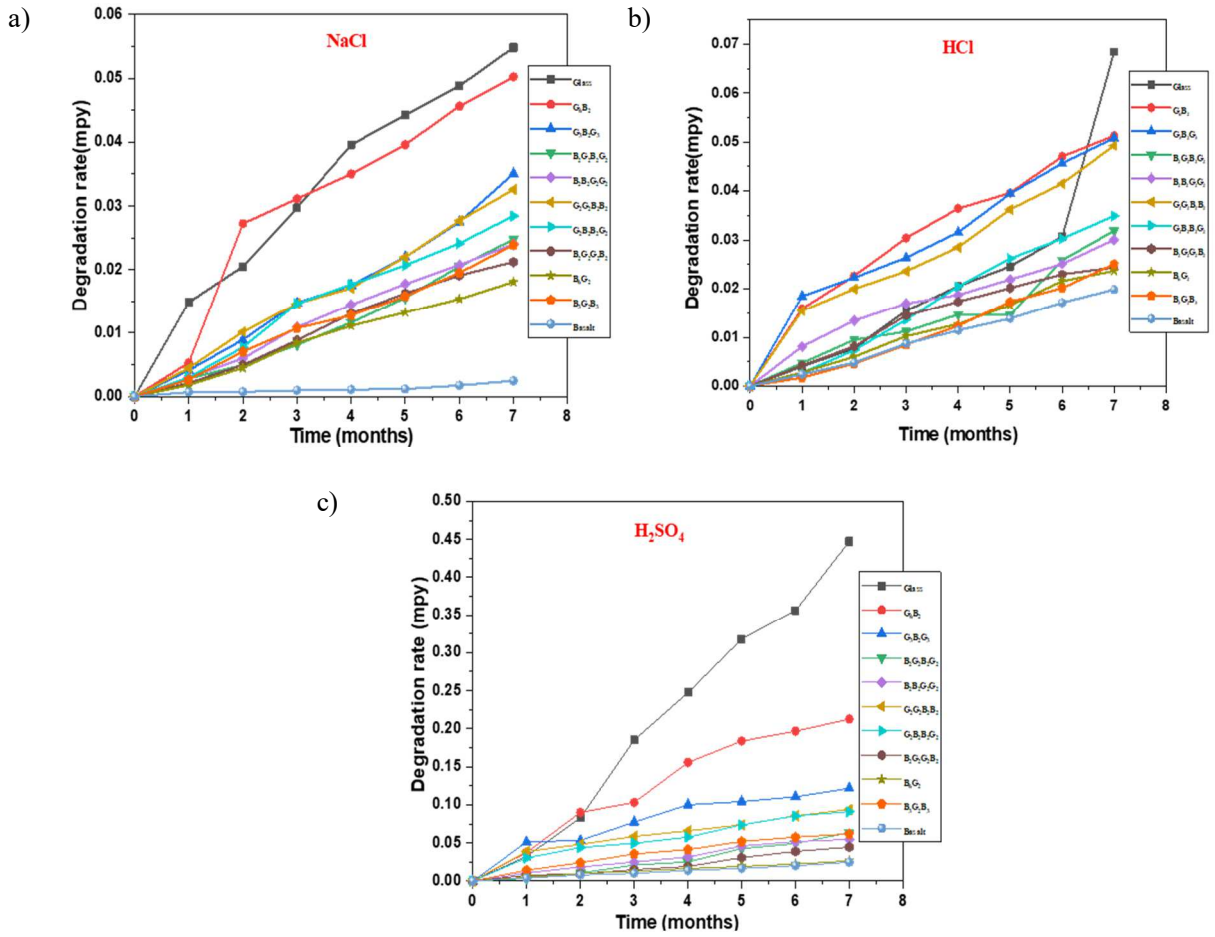

Fig. 5. Degradation rate of composite specimens with three solutions as a function of exposure time (a-c)

Figure 6 provides a visual representation of the surface morphological characteristics exhibited by both the pure and hybrid FRP pipe specimens after exposure to the 3.5 mol NaCl solution. Notably, the fiber surfaces have a granular structure, suggesting the occurrence of chemical reactions throughout the treatment process. Under highly alkaline conditions, it is evident that both the basalt and E-glass fibers exhibit similar deterioration features, characterized by a loss of strength and volumetric consistency. This degradation can be attributed to the interaction of Cl^- and NaOH reagents with the E-glass fiber web structure, leading to surface reactions and structural damage. Simultaneously, certain internal components of the E-glass fiber may migrate outward and deteriorate in the solution. Additionally, the alkali silicate present in the fibers may undergo hydrolytic reactions. The presence of Al_2O_3 in the fibers further compromises their chemical stability when exposed to alkali molecules. It is noteworthy that both the E-glass and basalt fibers are primarily composed of SiO_2. In the context of chemical treatment in an alkaline solution, the hydroxyl ions break the Si-O bonds, which constitute the primary framework of the fibers. Consequently, the strength of the fibers experiences a significant reduction following exposure to an alkaline solution. A great deal of research has been dedicated to investigating the behavior of glass fiber-reinforced materials in sodium chloride environments. Currently, there is considerable interest in the suitability of basalt fiber as an alternative material for structural reinforcement. This study specifically focuses on investigating the response of fibers to the external chemical environment, with particular emphasis on fiber fractures and their dynamics in the presence of sodium chloride. The research aims to shed light on the suitability of hybridizing glass and basalt fibers in FRP pipes that must withstand both mechanical loads and corrosive stresses, a critical concern in various industrial applications.

Initially, the surfaces of the E-glass, basalt, and hybrid FRP pipes appeared to be largely undamaged, with minor superficial imperfections like extrusion patches, which were likely a byproduct of the fabrication process. However, following the acid-immersion tests, these FRP pipe surfaces exhibited varying degrees of deterioration, influenced by the hybridization of the two types of fibers and the concentration of the acid used. Figures 7 and 8 provide an overview of the observed changes in the morphology of fiber surfaces during exposure to HCl and H_2SO_4 acids. Both the basalt and E-glass FRP pipes exhibited similar degradation behavior and fracture processes. However, it is crucial to highlight that the observed surface damage on the basalt FRP pipes occurred after 5 months of immersion, while the hybrid FRP pipes (composed of 50 % E-glass and

50 % basalt, as well as 75 % basalt and 25 % E-glass) exhibited surface damage after 4 months. Until this point, no cracks or damage were observed on the fiber surfaces. In contrast, the E-glass and hybrid FRP pipes (with a composition of 75 % E-glass and 25 % basalt) immersed for 2 months displayed numerous micro-cracks on the E-glass FRP surface. In other words, the basalt fiber exhibited crack formation at longer exposure times compared to E-glass. It is important to note that the degradation process is a time-dependent phenomenon, and the degradation of fiber strength should be studied over time. Additionally, after 5 months of immersion, the basalt, 50 % hybrid, and 75 % hybrid specimens exhibited spiral and axial cracks. This study developed a scenario for crack formation in basalt fiber based on SEM micrographs and the observed similarity in the fracture mechanisms in the, E-glass and hybrid FRP pipe specimens.

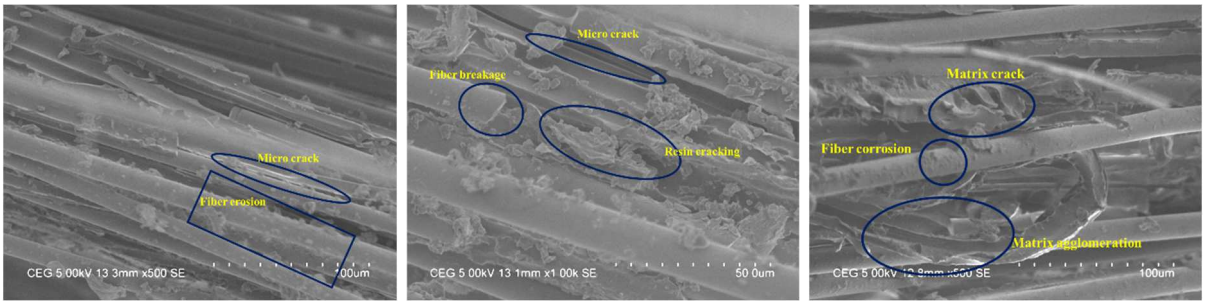

Fig. 6. SEM micrograph of NaCl-treated FRP pipe

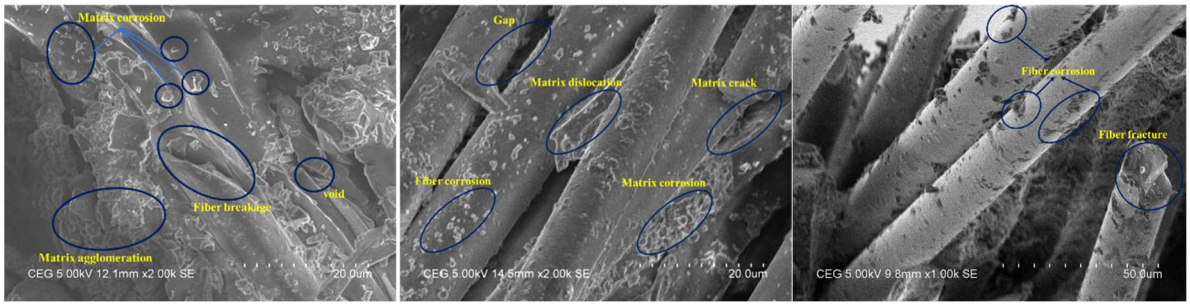

Fig. 7. SEM micrograph of HCl-treated FRP pipe

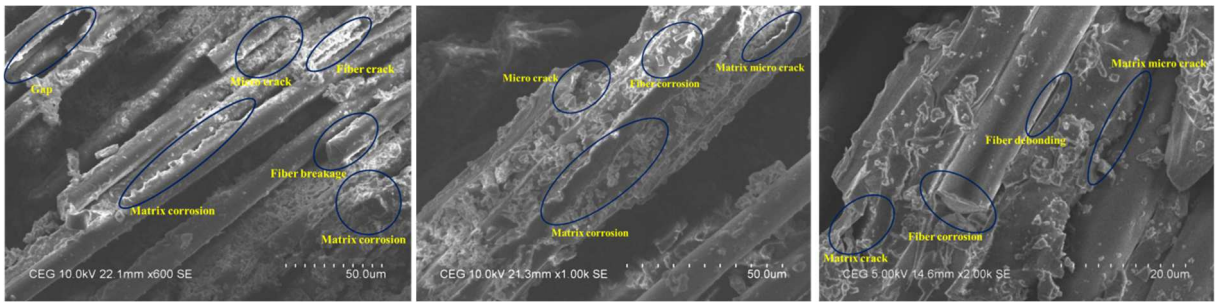

Fig. 8. SEM micrograph of H_2SO_4 treated FRP pipe

The occurrence of cracks on the surface of the FRP pipes can be attributed to two primary factors: residual stresses generated during the filament winding fabrication process and the shrinkage stress that arises at the interface between each layer surface and its core material. The process of ion transfer between the acid and the fiber composite layer during degradation induces shrinkage in the outer surface of the FRP pipes [32]. This shrinkage, coupled with variations in the mechanical properties between the intact inner core and the deteriorated outer surface, results in the development of three-dimensional stresses within the FRP pipes. Under these conditions, cracks tend to initiate from outer points on the FRP surface and propagate through the damaged area at specific pitch angles. In such cases, the lower strength of the degraded E-glass located in the middle layer of the hybrid FRP pipes exhibits superior performance compared to the other stacking sequences of the hybrid FRP pipes, where cracks primarily form in the axial direction of the FRP pipe. In most instances, a combination of axial, hoop, and spiral stresses is present. The SEM micrographs reveal that even after 5 months of degradation, the dominant cracks on the surfaces of the FRP pipes remain predominantly spiral in nature. Consequently, axial cracks were only observed on the surfaces of the E-glass and 75 % E-glass

hybrid FRP pipe specimens, while spiral cracks were the predominant mode of damage in the outer layers of most of the specimens.

Low-velocity impact analysis

Low-velocity impact tests were conducted on the pure E-glass fiber, pure basalt fiber, and 50:50 basalt-glass hybrid composite pipes at various impact energy levels (20 J, 30 J, and 40 J). The primary parameters used to evaluate the impact resistance included the maximum impact force, maximum deformation, and energy absorption capacity, which are presented in Table 5. The analysis involved dividing the load-time curve into two distinct regions, representing the damage initiation phase and the subsequent propagation of damage. During the initial phase of impact testing, damage occurs as the load increases and elastic strain energy accumulates in the impacted zone of the specimen, without significant failure. Observable changes in the load-time curves signify micro-damage events. Once the critical load is reached at the boundary of the first layer, signifying shear failure, the load begins to decrease, indicating the progression of damage. At this stage, the crack may spread catastrophically, leading to a persistent load drop, as evidenced by load fluctuations in the load-time curve, while still absorbing energy at lower loads. Figures 9a-c depict the load-time curves for the glass, basalt, and hybrid composite pipes subjected to impact testing. At the lowest impact energy of 20 J, the damage in the initial phase is minimal, with noticeable load-time curve variations associated with Hertzian failure. In the pure and hybrid FRP composite pipes, there is virtually no detectable damage at 20 J, and no signs of cracking on their front and inner surfaces, as revealed by ultrasonic scanning in Figure 10a. Nonetheless, as the impact energy increases to approximately 30 J and 40 J, the impact damage on the outer surface of the specimen becomes evident in Figure 10b and 10c using ultrasonic scanning. The specimen exhibits clear front-side fracture and substantial plastic deformation, along with a noticeable scratch, at these higher energy levels. The load initially rises upon contact, as indicated in the load-time curve, but this behavior persists until Hertzian failure occurs. The matrix cracking failure observed at the point of contact may be related to Hertzian failure. Nevertheless, the pipes maintain their structural integrity and can withstand the applied deformation.

TABLE 5. **Impact properties of pure and hybrid composite pipes**

Sample	Notation	Impact energy [J]	Peak load [kN]	Impact time [ms]	Maximum displacement [mm]	Absorbed energy [J]	Damaged area [mm^2]
1.	BFRP	20 J	5.055	2.34	3.576	14.598	25.158
		30 J	6.100	2.42	4.627	24.206	77.310
		40 J	6.371	2.33	6.348	34.199	93.88
2.	HFRP	20 J	4.919	2.45	3.632	14.721	27.354
		30 J	5.738	2.51	5.216	25.192	80.011
		40 J	5.850	3.03	7.079	34.199	97.63
3.	GFRP	20 J	4.882	2.41	3.694	14.844	45.51
		30 J	5.161	2.76	5.883	24.777	84.692
		40 J	5.489	2.85	7.418	35.369	120.91

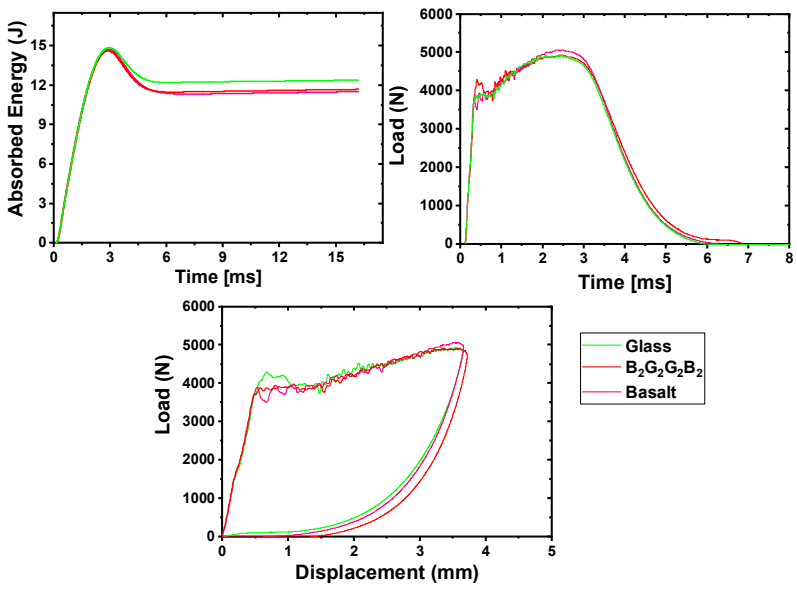

Fig. 9a. Impact properties of 20 J load-time, load-displacement and absorbed energy-time curve

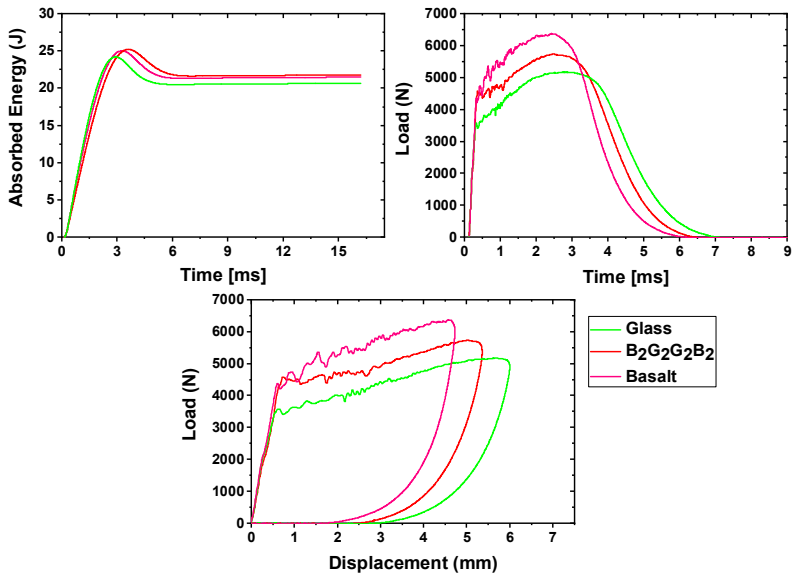

Fig. 9b. Impact properties of 30 J load-time, load-displacement and absorbed energy-time curve

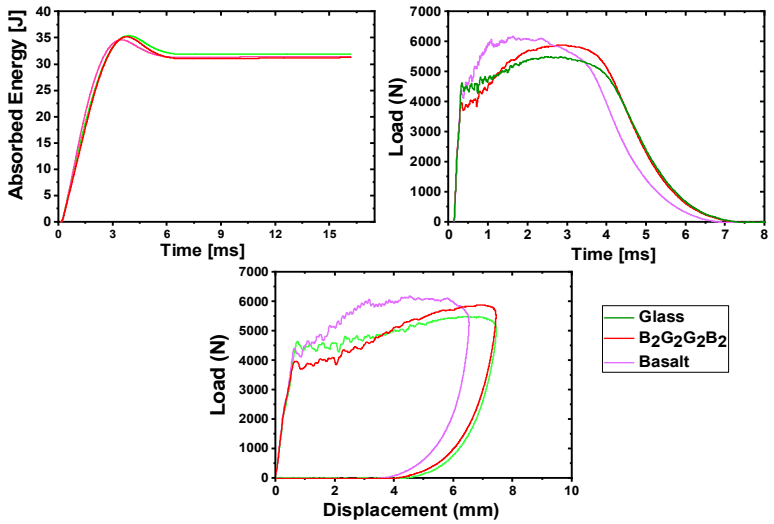

Fig. 9c. Impact properties of 40 J load-time, load-displacement, and absorbed energy-time curve

The absorbed energy vs. time curve provides valuable insights into the energy absorption behavior of composite specimens during impact testing. In this curve, the energy absorbed up to the peak load is primarily attributed to elastic deformation, resulting in a linear increase. However, beyond the peak load, the energy absorption exhibits a non-linear rise, indicating that damage occurring after the peak load is primarily inelastic in nature. This transition from linear to non-linear behavior is critical as it reflects the toughness and durability of the composites, making the absorbed energy a crucial parameter to evaluate impact resistance and damage capacity. The quantification of absorbed energy involves calculating the area under the load-displacement curves and comparing it with results obtained from the impact instrument. Each tested condition is explicitly represented by the load-displacement curve from the impact analyses. Figure 9a, 9b, and 9c presents the load-displacement curves for the basalt, E-glass, and hybrid FRP pipes subjected to impact energies of 20, 30, and 40 J. Notably, while the maximum impact load and maximum displacement of the basalt specimen were slightly higher than those of the E-glass specimen, the basalt specimen exhibited greater energy absorption. This result may seem counterintuitive given the fact that basalt fibers are generally considered to be more brittle compared to E-glass fibers, implying a potential inability to withstand impacts without significant dampening, which is indicative of poor toughness properties. In contrast, the E-glass specimen displayed higher damage, resulting in more visible cracks and delamination areas. Specifically, the pure E-glass specimen exhibited delamination damage as compared to the pure basalt sample. This observation highlights the hybrid FRP pipe's capacity to enhance energy absorption in interlaminar damage scenarios rather than intralaminar damage, contributing to greater energy absorption compared to the E-glass sample.

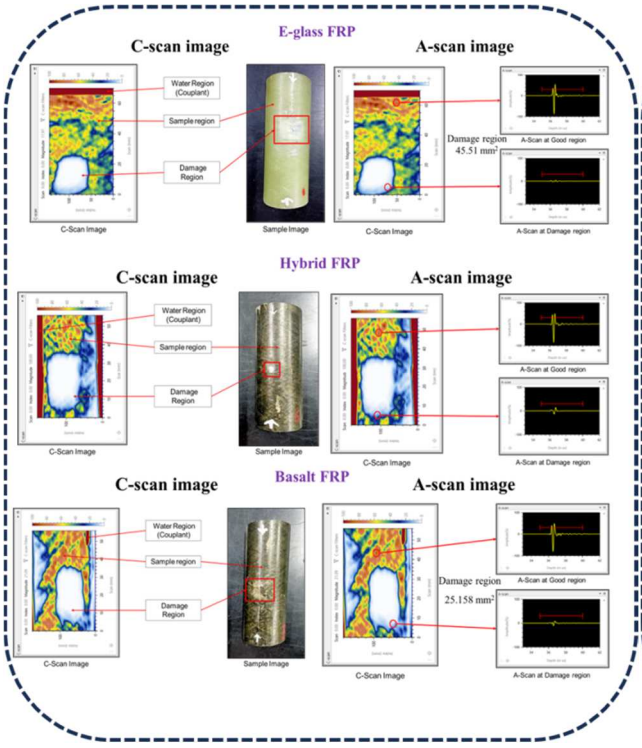

Fig. 10a. A-C scan damage analysis of 20 J E-glass, basalt and $B_2G_2G_2B_2$ hybrid FRP composite

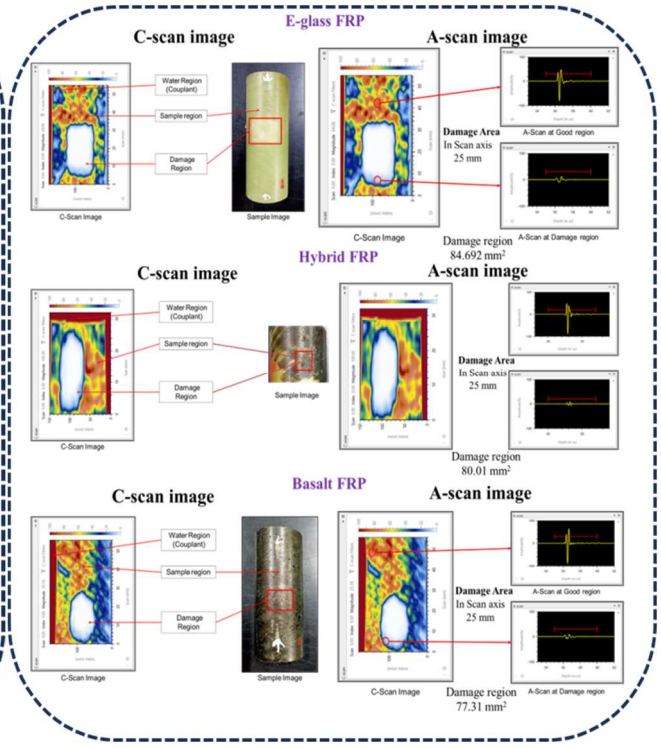

Fig. 10b. A-C scan damage analysis of 30 J E-glass, basalt and $B_2G_2G_2B_2$ hybrid FRP composite

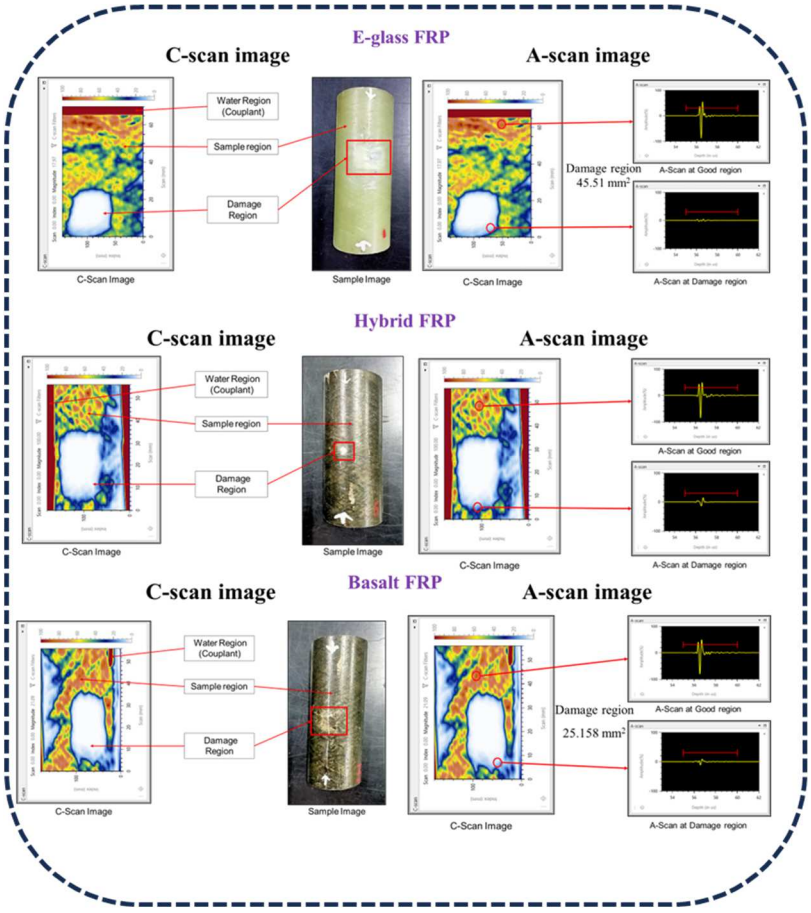

Fig. 10c. A-C scan damage analysis of 40 J E-glass, basalt and $B_2G_2G_2B_2$ hybrid FRP composite

The load-time and load-displacement curves exhibit variations due to different failure mechanisms, including the initiation point and gradual propagation of delamination at multiple distinct levels. Moreover, the damping behavior of the composite materials and the wide frequency range during the impact tests can influence the outcomes. The bending stiffness of and cumulative damage on the pipe specimens were notably affected by the absence of internal pressure during impact loadings. Specifically, in the case of the 30 J impact energy scenario, the stacking sequence with E-glass fiber on the interior demonstrated an improved damage response. The alternation of more ductile fibers on the impacted side resulted in superior impact resistance, consistent with existing research. Concerning the energy-absorbing mechanism, the behavior of the hybrid pipes differed noticeably from E-glass fiber, with the basalt fiber specimens showing significant improvement. Similar variations, along with more severe damage, were observed in the 40 J load-displacement plots. A significant observation from the load-displacement curve was an increase in loading until a specific point before a sudden degradation, particularly evident in the E-glass fiber specimens. This increase in energy absorption can be attributed to the progressive failure and subsequent collapse occurring within the fibers of the constituent materials of the pipes. In contrast, the E-glass composites displayed concentrated damage in the impact zone, leading to reduced energy absorption capacity compared to areas with distributed damage.

A substantial portion of low-velocity impact damage remains invisible to the naked eye, significantly compromising the structural efficiency of the pipe materials. Therefore, estimating the damaged area becomes highly valuable. In this study, ultrasonic C-scan images were analyzed using Image J software, a Java-based image processing tool, to quantify the extent of damage in the pure E-glass, basalt, and hybrid FRP pipes, enabling meaningful comparisons. The software provides precise measurements of the damaged areas in composites and various other materials. For the hybrid composites, the outer layers consisting of basalt fibers distributed damage over a larger area, resulting in a more dispersed and less concentrated effect on the inner E-glass fibers. Consequently, incorporating 50 % glass fibers into the basalt fiber sample led to a decrease in the impact damage area of the hybrid FRP pipe compared to the E-glass fiber FRP pipe (20 J – 39.89 %, 30 J – 5.527 %, 40 J – 19.25 %). This arrangement enhances the toughness and leads to a higher energy absorption capacity compared to the pure E-glass fiber FRP pipe laminates. Specifically, the hybrid composites comprising 50 % basalt fiber as outer layers and 50 % E-glass fiber as inner layers exhibit superior energy absorption properties. In this study, the C-scan imaging technique was employed to detect damage on the outer surface of the composites by analyzing the propagation of sound waves in the tested pipes. This approach offers insights into the internal structure of the pipe through the reverberation of sound waves. Visual and graphical representations of the C-scan and A-scan results for the pure E-glass, basalt, and hybrid FRP composite pipes are provided in Figure 10a, 10b, and 10c. Observations derived from these images are categorized based on the behavior of waves as they propagate through the pipe thickness from right to left. These categories encompass waves exhibiting a high amplitude in undamaged sections, a decrease in wave amplitude when approaching a defect or damaged area, and a neutral curve at the damage zone where the wave amplitude is close to zero. The basalt-E-glass hybrid composites demonstrate superior impact resistance, while the E-glass FRP composites exhibit ductile deformation within the pipe, allowing damage to be distributed over a larger area. Consequently, these hybrid laminates effectively manage delamination and minimize the risk of collapse during perforation.

CONCLUSIONS

The experimental testing encompassed a comprehensive evaluation of FRP composite pipes comprising E-glass, basalt, and hybrid combinations. The conducted tests included a spectrum of assessments, including three-point flexural testing, immersion degradation evaluations utilizing NaCl, HCl, and H_2SO_4 solutions, and low-velocity drop weight impact testing conducted using three distinct impact energy levels (20 J, 30 J, and 40 J). The primary objective of this study centered on a meticulous exploration of the influence of diverse parameters, specifically the fiber content, fiber winding angle, and stacking sequences of the fiber layers.

The flexural behavior of the pure and hybrid basalt/E-glass FRP composite pipes was comprehensively investigated, focusing on the fiber content, and stacking sequences. The hybrid FRP pipes with the 50 % basalt fiber content in the outer layer showed remarkable resistance to bending loads, compared to the pure E-glass pipes and other hybrid pipes with different stacking sequences. These results highlight the potential of such hybrid pipes for structural applications requiring high bending strength. The study also revealed significant enhancement in the impact resistance of the basalt and hybrid FRP pipes. Increasing the proportion of basalt fiber in the hybrid pipes was associated with reduced damage during impact events. The arrangement of the fiber layers within the pipe structure influenced the impact resistance, with basalt on the impact-exposed side, leading to improved resistance across all the impact energy levels. Conversely, the incorporating basalt fiber on the exterior side reduced the impact resistance. Hybridization with a 50 % distribution of basalt and E-glass fibers showed superior energy absorption compared to the E-glass and other hybrid FRP pipes. Nonetheless, distinct failure mechanisms were observed in the A- and C-scan analysis across different impact

energy levels. The investigation into the degradation behavior of the pure and hybrid FRP composite pipes exposed to NaCl, HCl, and H_2SO_4 solutions unveiled intriguing findings. The specific stacking sequence featuring an outermost basalt layer and a 50% distribution of the two different fibers, demonstrated remarkable resistance against degradation. When subjected to alkaline solutions, these composite pipes exhibited relatively smaller affected zones, resulting in fewer instances of damage. Nevertheless, under the influence of acid solutions, particularly H_2SO_4, the affected zones expanded significantly, leading to heightened levels of damage within the same timeframe. An extensive analysis of the failure mechanisms observed in the treated composite pipe specimens, including phenomena such as microcracks, fiber-matrix degradation, matrix debonding, and fiber fracture, was conducted using SEM.

REFERENCES

[1] Olarewaju A.J., Mannan M.A., Kameswara R.N.S.V., Response of Underground Pipes to Blast Loads, INTECH Open Access Publisher 2012, DOI: 10.5772/29101.

[2] Toh W., Tan L.B., Tse K.M., Giam A., Raju K., Lee H.P., Tan V.B.C., Material characterization of filament-wound composite pipes, Composite Structures 2018, 206, 474-483, DOI: 10.1016/j.compstruct.2018.08.049.

[3] Selmy A.I., Elsesi A.R., Azab N.A., Abd El-baky M.A., In-plane shear properties of unidirectional glass fiber (U)/ random glass fiber (R)/epoxy hybrid and non-hybrid composites, Composites Part B: Engineering 2012, 43(2), 431-438, DOI: 10.1016/j.compositesb.2011.06.001

[4] Maziz A., Tarfaoui M., Rechak S., Nachtane M., Gemi L., Finite element analysis of impact-induced damage in pressurized hybrid composites pipes, International Journal of Applied Mechanics 2021, August, 13, 07, DOI: 10.1142/s1758825121500745.

[5] Khalili S.M.R., Daghigh V., Eslami Farsani R., Mechanical behavior of basalt fiber-reinforced and basalt fiber metal laminate composites under tensile and bending loads, Journal of Reinforced Plastics and Composites 2011, April, 30, 8, 647-659, DOI: 10.1177/0731684411398535.

[6] Mingchao W., Zuoguang Z., Yubin L., Min L., Zhijie S., Chemical durability and mechanical properties of alkali-proof basalt fiber and its reinforced epoxy composites, Journal of Reinforced Plastics and Composites 2008, January, 27, 4, 393-407, DOI: 10.1177/0731684407084119.

[7] Mészáros L., Szakács J., Low-cycle fatigue properties of basalt fiber and graphene reinforced polyamide 6 hybrid composites, Journal of Reinforced Plastics and Composites 2016, September, 35, 22, 1671-1681, DOI: 10.1177/0731684416665176.

[8] Thirumavalavan K., Sarukasan D., Experimental investigation on multi-layered filament wound basalt/E-glass hybrid fiber composite tubes, Materials Research Express 2022, April, 9, 4, 045301, DOI: 10.1088/2053-1591/ac608d.

[9] Abd El-Baky M., Attia M., Flexural fatigue performance of hybrid composite laminates based on E-glass and polypropylene fibers, Journal of Thermoplastic Composite Materials 2018, February, 32, 2, 228-247, DOI: 10.1177/0892705717751020.

[10] Li B., Jiang Y., Koyama T., Jing L., Tanabashi Y., Experimental study of the hydro-mechanical behavior of rock joints using a parallel-plate model containing contact areas and artificial fractures, International Journal of Rock Mechanics and Mining Sciences 2008, March, 45, 3, 362-375, DOI: 10.1016/j.ijrmms.2007.06.004.

[11] Sarukasan D., Sudharson S., Thirumavalavan K., Prahadeeswaran M., Austin S.A., Experimental and Theoretical Analysis of $CaCl_2$ Liquid Desiccant System with Solar Regeneration, In: Recent Advances in Energy Technologies: Select Proceedings of ICEMT 2021 (19-33), Springer Nature Singapore, Singapore 2022.

[12] Gemi L., Köklü U., Yazman Ş., Morkavuk S., The effects of stacking sequence on drilling machinability of filament wound hybrid composite pipes: Part-1 mechanical characterization and drilling tests, Composites Part B: Engineering 2020, April, 186, 107787, DOI: 10.1016/j.compositesb.2020.107787.

[13] Pandian A., Vairavan M., Jebbas Thangaiah W.J., Uthayakumar M., Effect of moisture absorption behavior on mechanical properties of basalt fibre reinforced polymer matrix composites, Journal of Composites 2014, 2, 1-8, DOI: 10.1155/2014/587980.

[14] Koutsomichalis A., Kalampoukas T., Mouzakis D.E., Mechanical testing and modeling of the time-temperature superposition response in hybrid fiber reinforced composites, Polymers 2021, January, 13, 7, 1178, DOI: 10.3390/polym13071178.

[15] Muñoz E., García-Manrique J.A., Water absorption behaviour and its effect on the mechanical properties of flax fibre reinforced bioepoxy composites, International Journal of Polymer Science 2015, 6, 1-10, DOI: 10.1155/2015/390275.

[16] Chen D., Sun G., Meng M., Jin X., Li Q., Flexural performance and cost efficiency of carbon/basalt/glass hybrid FRP composite laminates, Thin-Walled Structures 2019, September, 142, 516-531, DOI: 10.1016/j.tws.2019.03.056.

[17] Chen D., Luo Q., Meng M., Li Q., Sun G., Low velocity impact behavior of interlayer hybrid composite laminates with carbon/glass/basalt fibres, Composites Part B: Engineering 2019, November, 176, 107191, DOI: 10.1016/j.compositesb.2019.107191.

[18] Sujon A.S., Habib M.A., Abedin M.Z., Experimental investigation of the mechanical and water absorption properties on fiber stacking sequence and orientation of jute/carbon epoxy hybrid composites, Journal of Materials Research and Technology 2020, September-October, 9, 5, 10970-10981, DOI: 10.1016/j.jmrt.2020.07.079.

[19] Gemi L., Investigation of the effect of stacking sequence on low velocity impact response and damage formation in hybrid composite pipes under internal pressure. A comparative study, Composites Part B: Engineering 2018, November, 153, 217-232, DOI: 10.1016/j.compositesb.2018.07.056.

[20] Farhood N.H., Karuppanan S., Ya H.H., Sultan M., Experimental investigation on the effects of glass fiber hybridization on the low-velocity impact response of filament-wound carbon-based composite pipes, Polymers and Polymer Composites 2020, July, 29, 7, 829-841, DOI: 10.1177/0967391120938181.

[21] Zhang C., Rao Y., Li Z., Li W., Low-velocity impact behavior of interlayer/intralayer hybrid composites based on carbon and glass non-crimp fabric, Materials 2018, December, 11, 12, 2472, DOI: 10.3390/ma11122472.

[22] Thirumavalavan K., Sarukasan D., Experimental investigation on multi-layered filament wound basalt/E-glass hybrid fiber composite tubes, Materials Research Express 2022, 9(4), 045301.

[23] Gemi L., Köklü U., Yazman Ş., Morkavuk S., The effects of stacking sequence on drilling machinability of filament wound hybrid composite pipes: Part-1 mechanical charac-

terization and drilling tests, Composites Part B: Engineering 2020, 186, 107787, DOI: 10.1016/j.compositesb.2020.107787.

[24] Gemi D.S., Şahin Ö.S., Gemi L., Experimental investigation of axial compression behavior after low velocity impact of glass fiber reinforced filament wound pipes with different diameter, Composite Structures 2022, January, 280, 114929, DOI: 10.1016/j.compstruct.2021.114929.

[25] Ding L., Liu Y., Liu J., Wang X., Correlation analysis of tensile strength and chemical composition of basalt fiber roving, Polymer Composites 2018, December, 40, 7, 2959--2966, DOI: 10.1002/pc.25138.

[26] Sarukasan D., Thirumavalavan K., Prahadeeswaran M., Muruganandhan R. Fabrication and mechanical characterization of jute-coir reinforced unsaturated polyester resin hybrid composites with various fiber size using compression moulding technique, International Journal of Recent Technology and Engineering (IJRTE) 2021, 10, 233-241.

[27] Gemi D.S., Şahin Ö.S., Gemi L., Experimental investigation of the effect of diameter upon low velocity impact response of glass fiber reinforced composite pipes, Composite Structures 2021, November, 275, 114428, DOI: 10.1016/j.compstruct.2021.114428.

[28] Wang J., GangaRao H., Liang R., Zhou D., Liu W., Fang Y., Durability of glass fiber-reinforced polymer composites under the combined effects of moisture and sustained loads, Journal of Reinforced Plastics and Composites 2015, July, 34, 21, 1739-1754, DOI: 10.1177/0731684415596846.

[29] Jáquez-Muñoz J.M. et al., Corrosion behavior of aluminum-carbon fiber/epoxy sandwich composite exposed on NaCl solution, Frontiers in Metals and Alloys 2023, September, 2, DOI: 10.3389/ftmal.2023.1258941.

[30] Vannan E., Vizhian P., Corrosion characteristics of basalt short fiber reinforced with Al-7075 metal matrix composites, Jordan Journal of Mechanical and Industrial Engineering 2015, January, 9, 2, 121-128.

Muhammad Faisal M.F., Hassan A., Gan K.W., Roslan M.N., Abdul Rashid A.H., Effects of sulphuric acid concentrations during solvolysis process of carbon fiber reinforced epoxy composite, Sains Malaysiana 2020, September, 49, 9, 2073-2081, DOI: 10.17576/jsm-2020-4909-05.

[31] Bazli M. et al., Durability of glass-fibre-reinforced polymer composites under seawater and sea-sand concrete coupled with harsh outdoor environments, Advances in Structural Engineering 2020, August, 24, 6, 136943322094789, DOI: 10.1177/1369433220947897.

